Structure and morphology of poly(∈-caprolactone)/chlorinated polyethylene (PCL/PEC1) blends investigated by DSC, simultaneous SAXS/WAXD, and elemental mapping by ESI-TEM

ARTICLE *in* MACROMOLECULES · DECEMBER 2006

Impact Factor: 5.8 · DOI: 10.1021/ma061265m

4 AUTHORS:

Tomás S Plivelic
Lund University
71 PUBLICATIONS **478** CITATIONS
SEE PROFILE

Silvana Navarro Cassu
Instituto de Aeronáutica e Espaço
20 PUBLICATIONS **155** CITATIONS
SEE PROFILE

Maria Do Carmo Gonçalves
University of Campinas
95 PUBLICATIONS **1,221** CITATIONS
SEE PROFILE

Iris L Torriani
University of Campinas
158 PUBLICATIONS **2,230** CITATIONS
SEE PROFILE

Structure and Morphology of Poly(ϵ-caprolactone)/Chlorinated Polyethylene (PCL/PECl) Blends Investigated by DSC, Simultaneous SAXS/WAXD, and Elemental Mapping by ESI-TEM

Tomás S. Plivelic,[†] Silvana N. Cassu,[‡] María do Carmo Gonçalves,[§] and Iris L. Torriani*[,†,||]

Laboratório Nacional de Luz Síncrotron (LNLS), Campinas, SP, Brazil, Centro Técnico Aeroespacial (CTA), São José dos Campos, SP, Brazil, Instituto de Química, UNICAMP, Campinas, SP, Brazil, and Instituto de Física "Gleb Wataghin", UNICAMP, Campinas, SP, Brazil

Received June 7, 2006; Revised Manuscript Received September 5, 2006

ABSTRACT: In this work, the structure and morphology of miscible blends of poly(ϵ-caprolactone) and chlorinated polyethylene with 48% chlorine weight content (PCL/PECl) were studied by differential scanning calorimetry (DSC), simultaneous small and wide-angle X-ray scattering (SAXS/WAXD), and electron spectroscopy imaging in the transmission electron microscope (ESI-TEM). A unique glass transition temperature was obtained in each blend. In addition to this, the heat capacity and the width of the glass transition did not have a linear behavior with blend compositions. These facts correlate with the presence of microheterogeneities originated from different local compositions and densities of interactions in each blend. A consistent picture of the mode of segregation of PECl in the blend was obtained. For higher concentration of PCL, the volume fraction of lamellar stacks in the samples decreased as a function of the PECl content, indicating preferential interfibrillar localization of the amorphous component. For lower PCL concentration, interespherulitic segregation was the dominant mode. Elemental maps of chlorine confirmed these results and also revealed changes in the concentration of this element depending on its localization in the microstructure of the system. Gradients of chlorine concentration were measured in larger amorphous regions of the 40/60 and 20/80 PCL/PECl blends. Calculations of the one-dimensional correlation function probed the reduction of the lamellar thickness of PCL when the quantity of PECl in the blend was increased. Such a tendency could be rationalized if the reduction of the fold surface free energy was a dominant factor in terms of the reduction of the degree of supercooling in the final crystal thickness.

Introduction

Polymer blends containing crystallizable components present a great variety of morphologies. The prediction and control of these morphologies as well as the understanding of the crystallization behavior during its processing will enable new materials to be developed. Upon crystallization of a two-component miscible blend in which one of them is crystallizable, the crystalline phase separates from the mixture. This liquid−solid-phase separation is different from the liquid−liquid phase separation and the miscibility generally still exists in the remaining amorphous phase.[1] Depending on the localization of the amorphous diluent, various types of morphologies may be created, commonly referred to as *interlamellar* (diluent between lamellae), *interfibrillar* (diluent between lamellar bundles or stacks of lamellae), and *interspherulitc* (diluent between spherulites) segregation. Different morphologies may coexist, leading to multiple locations of the amorphous diluent.[2]

It is difficult to predict the mode of segregation for a given blend.[3] Kinetic and thermodynamic factors need to be considered and every case may depend on composition, temperature and molecular weight involved. With regard to the kinetic factors one should consider the competition between the diffusion coefficient of the non (or less) crystallizable molecules of the blend and the crystal growth rate. From the thermodynamic point of view, the lower conformational entropy of the diluent molecules confined in the interlamellar regions and the crystallization driving force of the crystallizable segments in these regions (within the interlamellar zones) expels the diluent from the interlamellar zones. The polymer−polymer interaction described by the parameter χ (Flory−Huggins), competes with these two forces promoting interlamellar incorporation due to the favorable interaction that exists between the diluent and the amorphous fraction of the semicrystalline polymer in the interlamellar regions.

For weakly interacting systems, in which the glass transition temperature (T_g) of the amorphous polymer has bigger values than the T_g of the semicrystalline polymer, the diluent mobility at different crystallization temperatures determines its location. For $T_g \geq T_c$, the diluent is trapped between crystal lamellae whereas for low T_g, the molecules of the diluent can diffuse away from the crystal growth front and remain, at least partially, in interfibrillar regions.[4]

Among the different miscible semicrystalline/amorphous polymer blends with weak intermolecular interaction the poly(ϵ-caprolactone)/chlorinated polyethylene (PCL/PECl) blend is a very attractive system for study because of its large miscibility range depending on Cl content of PECl. The miscibility in the amorphous phase with chlorinated polyethylenes having chlorine contents of 36%, 42%, and 48% (by weight) were previously confirmed for all compositions by Bélorgey et al.[5] and Defieuw et al.[6] Poly(ϵ-caprolactone) are being investigated worldwide to extend its applications in the field of surgery (suture material, devices for internal bone fracture fixation), pharmacology (sustained drug delivery systems), and tissue engineering

* Corresponding author. E-mail: torriani@ifi.unicamp.br. Telephone: 55-19-3512-1117. Fax: 55-19-3512-1004.
[†] Laboratório Nacional de Luz Síncrotron (LNLS)-Campinas.
[‡] Centro Técnico Aeroespacial (CTA).
[§] Instituto de Química, UNICAMP.
[||] Instituto de Física "Gleb Wataghin", UNICAMP.

10.1021/ma061265m CCC: $37.00
Published on Web 12/24/2006

(scaffold for tissue regeneration).[7,8] This is mainly due to their good biocompatibility and variable degradability. Blending PCL with PECl can provide new possibilities for its application in the medical field.

The superstructure of the semicrystalline PCL/PECl blends has also been described using optical and electron microscopy and small-angle X-ray scattering (SAXS). The results point to localization of PECl mainly between fibrils for miscible blends rich in PCL, and in the interspherulitic spaces, for the other compositions.[6]

A consistent picture of the segregation mode of PECl in the blend is possible if different techniques are applied on identical bulk samples. SAXS is an excellent tool to characterize the system in the lamellar scale and combined simultaneous SAXS/WAXD experiments lead to the correct association of the calculated morphological parameters.[9,10] However, the spherulite architecture is much more complex than that of a simple lamellar structure model. The micrometer scale structure can be well described by optical and electron microscopy whereas the finer morphological details can be obtained by transmission electron microscopy (TEM).[11] The analysis of the semicrystalline regions observed by the latter technique could be compared with X-ray scattering experiments to describe the blend morphology and particularly the amorphous component localization. In the case of blends with low degree of crystallinity, TEM analysis is essential to characterize the lamellar morphology because lamellar X-ray scattering may be too weak. Furthermore, amorphous phase domains present in the sample will grow in size (outside SAXS scale detection) when the amorphous fraction added to the blend increases. TEM and especially electron spectroscopy imaging (ESI) can give valuable and unambiguous information in size and elemental composition of this phase. ESI-TEM technique has the additional advantage of not requiring any special sample preparation (as staining or etching) avoiding the possibility of imaging artifacts.

Other miscible semicrystalline/amorphous polymer blends with weakly intermolecular interaction offer valuable morphological and structural information (PEEK/PEI;[12,13] PEO/PVAc and PEO/PMMA[4,10,14]). To the best of our knowledge, only the PEEK/PEI blends have been studied in detail by electron microscopy of bulk samples.[15] Blends of PCL with a variety of amorphous polymers are miscible[16] but TEM analyses are scarce and nonexhaustive.[6,11,17]

A combination of simultaneous SAXS/WAXD experiments using synchrotron radiation, DSC (differential scanning calorimetry) measurements and ESI-TEM analysis allowed us to follow the changes of the morphology of the PCL/PECl blends as a function of its compositions. We report the calculation of structural and thermal parameters for all the compositions, which gives us a further insight on the lamellar and interfibrillar morphology of the binary blends, providing evidence for the extralamellar segregation of the amorphous component and adding quantitative details to the existing information on this subject.

Experimental Section

1. Materials and Sample Preparation. The homopolymers poly(ϵ-caprolactone) (PCL) $M_w = 65\,000$ g/mol, $M_w/M_n = 1.44$, and chlorinated polyethylene (PECl) with 48% Cl weight content, $M_w = 43\,250$ g/mol, $M_w/M_n = 1.7$, were obtained from Aldrich Co. Polymer average molecular weights were determined by gel-permeation chromatography (GPC) performed at 40 °C in tetrahydrofuran (THF) using an Agilen 1100, PL gel mixed B columns with a refractive index detector. Polystyrene was used for calibration. C^{13} solid-state NMR of pure PECl was used to prove that the chlorine atoms have a random distribution along the polyethylene backbone (results not shown). The solvent-casting method was employed to prepare films of the homopolymers and blends, mixing the desired mass fractions of PCL and PECl. Toluene was the common solvent of the homopolymers. The prepared blend compositions (PCL/PECl) were as follows: 90/10, 80/20, 70/30, 60/40, 50/50, 40/60, 30/70, 20/80, and 10/90. The samples were dried at room temperature for 1 week. Subsequently, they were dried for 15 days at $T = 35$ °C in a vacuum stove. Starting at $T = 35$ °C the melting of the samples were reached with a heating rate of 5 °C/h keeping the samples at $T = 80$ °C for 10 min. After a rapid quenching from $T = 80$ °C down to $T = 35$ °C the samples were annealed keeping them at this temperature for 22 days. The same samples were used for DSC, SAXS/WAXD and TEM measurements.

2. Differential Scanning Calorimetry (DSC). The calorimetric measurements were made on a MDSC 2910 TA differential scanning calorimeter in argon atmosphere. Samples of about 10 mg were placed in the DSC pan. The samples were first stabilized at 0 °C, then they were heated to 150 °C at a rate of 20 °C/min (first heating scan) and subsequently kept at that temperature for 5 min. The cooling scan was made at the same rate from +150 to −120 °C. Finally, the second heating scan was made up to 150 °C at the same rate. The midpoint of the slope change of the heat flux plot as a function of the temperature obtained in the second heating scan was taken as the glass transition temperature (T_g). The melting temperature was taken as the minimum of the endothermic peak in the two heating scans (T_{m1} and T_{m2}) whereas the enthalpy of fusion (ΔH_f) was evaluated from the area of the corresponding melting peaks. The crystallization temperature (T_c) was taken as the maximum of the exothermic peak (during the cooling scan).

3. Small-Angle X-ray Scattering and Wide-Angle X-ray Diffraction (SAXS/WAXD). Simultaneous SAXS/WAXD experiments were performed at the D11A-SAXS beamline of the Brazilian Synchrotron Light Source (LNLS), using a wide angle chamber with image plate detection for the wide angle range and a position sensitive detector for the small angle region.[18] The wavelength used was 1.7433 Å. Small angle scattering was registered for values of the scattering vector q ($q = (4\pi \sin\theta)/\lambda$; 2θ = scattering angle) from $q_{min} = 0.01(Å^{-1})$ to $q_{max} = 0.3(Å^{-1})$. The wide angle diffraction peaks were detected between $2\theta = 15°$ and $2\theta = 80°$. α-Al_2O_3 was used as a calibration standard for peak position.

The melted state of each blend was also measured in simultaneous SAXS/WAXD experiments heating the samples in a specially designed hot stage cell (THM 600, Linkam Ltd., see Bras et al.[19] and Plivelic et al.[20] for specific details of the setup). Analogous results (in the coincident q, 2θ range) were obtained in both setups. For these measurements, the samples were compressed and sealed in a modified aluminum DSC pan with mica windows (25 μm thickness).

4. Transmission Electron Microscopy (TEM). Ultrathin sections of bulk specimens (approximately 50 nm thick) were obtained at −90 °C using a Reichert FCS ultramicrotome fitted with a diamond knife. The morphology and elemental distribution in the films were examined in a Carl Zeiss CEM 902 transmission electron microscope, equipped with a Castaing-Henry energy filter spectrometer within the column.

Elemental images were observed for chlorine, the characteristic element in PECl, using monochromatic electrons with an energy-selecting slit of 15 eV. The energy-selecting slit was set at 200 eV, which corresponds to the chlorine $L_{2,3}$-edge. To make sure that sample thickness was adequate for elemental mapping, the image contrast inversion was monitored, as the energy loss of the electrons used for energy-filtered imaging was changed from 0 to 20 eV. The images were recorded using a Proscan high-speed slow-scan CCD camera and digitized (1024 × 1024 pixels, 8 bits) using the AnalySis software. Further image processing was done using the software Image-Pro Plus 4.5.

Results and Discussion

1. Differential Scanning Calorimetry (DSC). In Figure 1a, we show the thermograms obtained in the second heating cycle

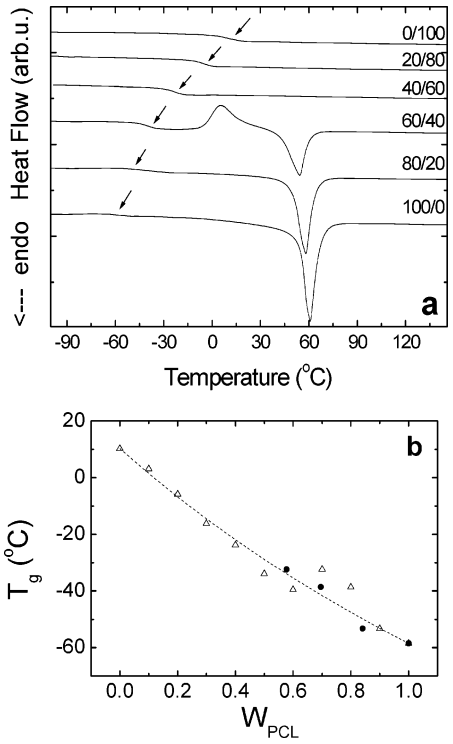

Figure 1. (a) DSC thermograms of the homopolymers, PCL and PECl, and some PCL/PECl blend compositions in the second heating scan. The arrows indicate the T_g. (b) Glass transition temperature T_g: experimental (empty triangle); T_g vs calculated amorphous composition (Fernandes et al.[22]) (full dots); predicted T_g values using Fox equation (dotted line).

for the homopolymers and some of the blends under study. The arrows indicate the glass transition temperatures, which are plotted in Figure 1b as a function of PCL weight fraction. All blends showed one T_g value that depends on the composition. The T_g values found are in the range from −58.5 ($T_{g,PCL}$) to +10.3 °C ($T_{g,PECl}$). This fact indicates that the amorphous phase of both components is miscible in all the compositions studied.

The behavior of the glass transition temperature of the blends can be well described by the Fox equation:[21]

$$\frac{1}{T_g(\text{blend})} = \frac{W_{PECl}}{T_{g,PECl}} + \frac{W_{PCL}}{T_{g,PCL}} \tag{1}$$

where T_g (blend) is the glass transition temperature for the blend and W_{PECl} and W_{PCL} are the mass fractions of PECl and PCL in the blend, respectively.

The experimental and calculated T_g values are shown in Figure 1b (empty triangles and dotted line, respectively). We note, though, that the points corresponding to the samples with a higher crystalline fraction (70% or more PCL mass fraction) have values higher than predicted from eq 1. Because of the significant crystallization of PCL in these blend compositions, the weight fraction of PCL in the amorphous phase, W'_{PCL}, is not equal to its overall weight fraction in the blend W_{PCL}. The actual composition of the amorphous phase can be corrected by the expression[22,23]

$$W_{PCL}' = \frac{W_{PCL} - X_c}{1 - X_c} \tag{2}$$

where X_c is the degree of crystallinity of the blend calculated from the DSC measurements:

$$X_c = \frac{\Delta H_f}{\Delta H_f^\circ} \tag{3}$$

ΔH_f° is the enthalpy of fusion for the 100% crystalline PCL sample (ΔH_f° = 136 J/g[24]) and ΔH_f is the enthalpy of fusion of the blend.

The full dots in Figure 1b represent the T_g values vs the real amorphous fraction in the blend (obtained from eq 2). Since this plot is well fitted by the Fox equation, in which the interaction between the components is not considered, the T_g behavior of PCL/PECl blends suggests that the interaction parameter χ must be close to zero. This result is coherent with previous reports.[5,6] However, based on the data obtained in this work, the Flory−Huggins interaction parameter cannot be determined without ambiguity.

More details on the microheterogeneities and densities of interactions of the amorphous phase could be deduced from the behavior of the heat capacity change (ΔC_p) and the glass transition width (Δw) with blend composition.

The ΔC_p can be associated with the change of degrees of freedom of the polymer chains at the glass transition region resulting from free volume changes in this region. Ideal mixtures resulting from the random mixing of molecules that have the same size and shape and in which the intermolecular forces between pairs of like segments of each type, as well as between unlike segments, are all equivalent. Additivity of volume is expected for ideal mixtures, and in this case, ΔC_p should exhibit a linear dependence on blend composition. In this work, the values of ΔC_p were obtained from the height of the glass transition in the DSC plots, normalized by the heating rate. ΔC_p behavior as a function of the mass fraction of PCL in the PCL/PECl blends is displayed in Figure 2a. In this graph, the *x*-axis was not corrected for PCL crystallinity. The curve profile clearly indicates the nonadditivity of this system, suggesting the presence of specific interactions, which may be responsible for the miscibility of the PCL/PECl blend in the amorphous phase. Changes in the conformational orientation or chain packing in the amorphous phase could cause larger ΔC_p values compared to those of the homopolymers. A similar ΔC_p behavior was also observed for miscible PVA/PVP and PMMA/SAN blends[25,26] in which the deviation from linearity was explained by the presence of polymer−polymer specific interactions.

The width of the glass transition may reflect the magnitude of local compositional fluctuations in polymer blends.[27] The Δw values, obtained from the difference between the onset and endset of the glass transition process, are shown in Figure 2b as a function of W_{PCL}. Apart from PECl having bigger Δw than the PCL homopolymer, the deviation from a linear behavior with blend composition is more pronounced for blends with higher PCL content. A local maximum value, (close to that obtained for PECl, Δw = 45 °C), is observed for the 70/30 PCL/PECl blend, suggesting that specific interactions are more effective for this composition. The broadening of the vitreous transition in miscible systems is related to local composition fluctuations. The existence of microenvironments in blends containing up to 60% PCL may be the result of specific interactions between the chains in the amorphous phase and in the amorphous−crystalline interphase. The chains belonging to each microenvironment present specific structural relaxation, thus causing the broadening effect of the glass transition.[28]

Table 1 describes the melting temperature dependence with PCL content in the blend for the two heating cycles (T_{m1} and T_{m2}). In both scans we observe only one melting peak and a reduction of the melting temperatures with the increase of PECl

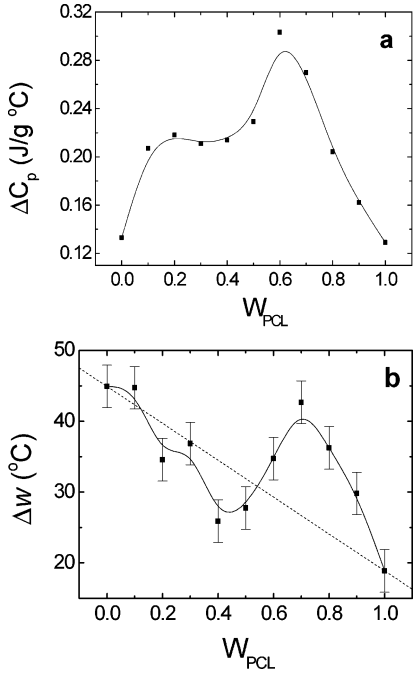

Figure 2. (a) Heat capacity changes (ΔC_p) in the glass transition region and (b) glass transition width (Δw) for PCL/PECl blends. Dashed line represents a linear behavior of Δw as a function of blend composition.

Table 1. Melting Temperatures, T_{m1} and T_{m2}, for the Two Heating Cycles and Crystallization Temperature, T_c, Obtained in the Cooling Scan

sample (PCL/PECl)	T_{m1} (°C)[a]	T_{m2} (°C)[a]	T_c (°C)[b]
100/0	67.9	60.8	26.3
90/10	63.6	57.7	18.9
80/20	64.9	58.1	13.6
70/30	62.4	55.4	5.9
60/40	62.7	54.3	
50/50	60.1	51.2	
40/60	60.6		
30/70	60.8		
20/80	56.0		

[a] T_{m1} and T_{m2} = melting temperatures obtained in the first and second heating cycles, respectively. [b] T_c = crystallization temperature obtained in the cooling scan.

in the blend. Given the fact that the blends were prepared by solvent casting and previously annealed at $T = 35$ °C (which favored the crystallization of PCL), the values of T_{m1} are higher than those of T_{m2} and melting peaks appear for higher concentrations of PECl in the first heating cycle. Melting temperatures are observed for samples with up to 80% PECl in the first heating cycle and for samples with up to 50% PECl in the second heating cycle. Compared with previous results on this blend,[5] crystallinity is not detected in all compositions studied in the present work. The difference may come from the fact that the PCL molar mass used in this work is higher than the one used in the literature cited above ($M_w = 20\,000$ g/mol).

The crystallization temperature (T_c) during the cooling scan decreases with the increase of the amorphous phase in the blend, and becomes undetectable by DSC for PECl mass fractions higher than 30%. For the PCL/PECl 50/50 and 60/40 blends, the exothermic peak is detected only during the (second) heating scan (see Figure 1a; the 50/50 curve is not shown).

The T_c reduction with blend composition indicates that the overall crystallization rate of PCL decreases with increasing PECl content. This fact can be a consequence of the increased content of the component with higher T_g value. Therefore, this delayed crystallization process can be correlated with the molecular mobility in the blend.

Table 2. Degree of Crystallinity of the Blends and PCL Obtained from DSC from the First Heating Cycle (X_c and $X_{c,PCL}$) and from WAXD (X_c^{WAXD}) Measurements

sample (PCL/PECl)	X_c (%)[a]	$X_{c,PCL}$ (%)[a]	X_c^{WAXD} (%)[b]
100/0	56.4	56.4	55.8
90/10	48.9	54.4	50.0
80/20	44.2	55.3	43.6
70/30	38.3	54.7	40.5
60/40	30.8	51.3	28.9
50/50	23.0	45.9	27.3
40/60	20.0	50.0	18.2
30/70	15.6	51.9	12.7
20/80	10.5	52.7	6.0

[a] X_c and $X_{c,PCL}$ = degree of crystallinity of the blend and PCL, obtained from DSC from the first heating cycle (eqs 3 and 4). [b] X_c^{WAXD} = degree of crystallinity of the blend obtained from WAXD measurements (eq 8).

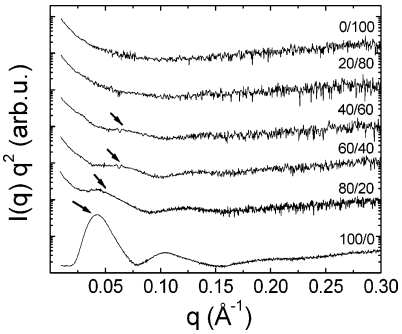

Figure 3. Lorentz-corrected SAXS plot for some of the PCL/PECl samples analyzed. Black arrows indicate the principal correlation peak associated with the lamellar morphology. A significant increase in low q intensity is noted for all samples with PECl content.

The results of the degree of crystallinity of the blend (X_c) and PCL ($X_{c,PCL}$) obtained from the first heating cycle are shown in Table 2. $X_{c,PCL}$ was calculated from the equation:

$$X_{c,PCL} = \frac{X_c}{W_{PCL}} \tag{4}$$

As expected, the degree of crystallinity, X_c, decreases due to the dilution effect of PECl. Meanwhile, $X_{c,PCL}$ remains practically constant, around 50%, for the first heating cycle of DSC in all compositions.

2. Small-Angle X-ray Scattering. The small angle scattering curves were normalized by the integrated incident beam intensity and sample absorption. In a $I(q)q^2$ vs q curve (Lorentz plot) the characteristic peaks associated with the lamellar periodicity are clearly defined in the experimental curves for the homopolymer PCL and for the blends with composition $W_{PCL} > 0.2$. (see Figure 3).

It is clear from the figure that the position of the first maximum is progressively shifted to higher q when PECl is increased in the blend composition. For an ideal lamellar structure, the position of this maximum (q_m), gives an estimation of the average long period, which can be obtained from the relation $L = 2\pi/q_m$. It should be mentioned that the existence of a distribution of layer thickness may have an influence on the real values of L calculated using this relation. Nevertheless, the increase of q_m values indicates the reduction of the long period with blend composition. Since the average long period, L, is the sum of the crystalline and amorphous components of an ideal structure ($L = l_c + l_a$) the observed reduction in the long period, does not permit to single out which is the precise

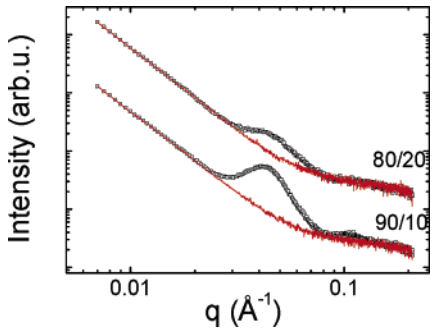

Figure 4. SAXS curves for the crystallized (*as prepared*) samples (empty squares) and melted blends (continuous red line) for the PCL/PECl 90/10 and 80/20 compositions, normalized by matching the tail end of the curves. The signal coming from the lamellar morphology is the only significant difference between the two states.

structural change when the weight fraction of PECl is increased in the blend.

For the low q values ($q \leq 0.025$ Å^{-1}), a marked increase in the scattered intensity for blends with higher PECl content is observed. To identify the most significant effect that contributes to the SAXS curves in this low q range, the samples were heated to its melting temperature and the SAXS curves were recorded during the process. The curves corresponding to the crystallized (as prepared) and melted state are shown in Figure 4 for the PCL/PECl blends 90/10 and 80/20. No significant intensity remains after subtraction of the melted state curves except the contribution of the lamellar morphology. This fact proves that the low q intensity represents a contribution from the amorphous state of the blend in which composition fluctuations and contrast variation will produce a different response for each composition. Consequently, the curves corrected by subtraction of the melted state curves contain only the signal needed to study the morphology of the crystallized state for each composition of the blend, via correlation function calculations.

To extract the morphological parameters of an ideal two-phase structure, we calculated the normalized one-dimensional correlation function, $CF(r)$, as proposed by Goderis et al.[29] as

$$CF(r) = \frac{1}{Q_{id}} \int_0^\infty (I(q) - I_m - I_b) q^2 \cos(qr)\, dq \qquad (5)$$

where I_m is the intensity of the melt pattern, I_b is the intensity due to the electron density fluctuations (in both phases) and Q_{id}, calculated for each blend, is a constant whose value corresponds to the y intercept of the linear fit obtained for the initial part of the integral function in eq 5.[30] Subtraction of I_m also eliminates the parasitic scattering contribution from the instrumental setup. Figure 5 shows the correlation functions obtained for some of the samples studied.

The normalized one-dimensional correlation function gives the thickness of each of the phases (l_1 and l_2) but the assignment of any of these parameters to the crystalline or amorphous component has to be determined with the help of other experimental observations. The comparison between the bulk degree of crystallinity of the blend, Φ_c, (calculated from WAXD or DSC measurements) and the linear degree of crystallinity within the lamellar stacks (χ_{cl}) allows this type of identification provided one of the ratios $l_i/L (i = 1,2)$ is bigger and the other one smaller than Φ_c. χ_{cl} is always bigger than or equal to Φ_c because not all the morphology of the blends is necessarily lamellar. Both crystallinity parameters were calculated from the equations:

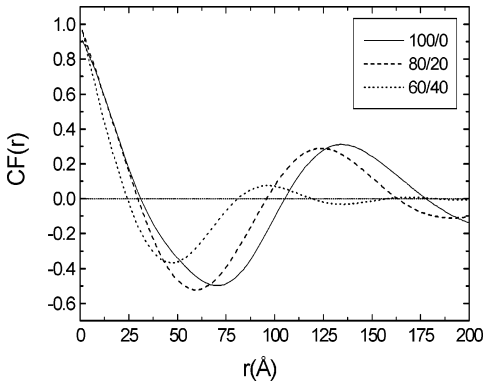

Figure 5. Normalized one-dimensional correlation function for some PCL/PECl blend compositions: 100/0, 80/20, and 60/40. The reduction of the long period (maximum in the *CF* curve) when more PECl is added in the blend is clearly observed.

$$\Phi_c = \frac{X_c/\rho_c}{X_c/\rho_c + (W_{PCL} - X_c)/\rho_a + (1 - W_{PCL})/\rho_{PECl}} \qquad (6)$$

$$\chi_{cl} = \frac{l_c}{L} \qquad (7)$$

where eq 6 was derived by Huo et al.[31] for a generic semicrystalline/amorphous blend. ρ_c and ρ_a are the densities of 100% crystalline and amorphous PCL[32] ($\rho_c = 1.194$ g/cm^3, $\rho_a = 1.095$ g/cm^3) and ρ_{PECl} is the density of PECl[33] ($\rho_{PECl} = 1.16$ gr/cm^3). For the PCL and the 90/10 and 80/20 blends l_c was chosen using the criteria mentioned above. For the other compositions, both l_i/L are bigger than Φ_c and the values of l_c were assigned by assuming a monotonic behavior of this parameter. The lamellar parameters as a function of blend composition are shown in Figure 6.

The average long period and the lamellar thickness show an almost monotonic decrease when more PECl is added to the blends. For the interlamellar amorphous thickness an initial increase is followed by a slight decrease for $W_{PCL} \leq 0.8$.The blend composition parameters that describe the dependence of the linear and bulk degree of crystallinity are listed in Table 3. In these sample compositions, no significant changes are observed in the linear degree of crystallinity within the lamellar stacks where as, a systematic decrease is noted for Φ_c and Φ_c/χ_{cl}.

3. WAXD. Diffractograms were obtained for the complete set of samples under study, and are shown in Figure 7. The principal X-ray diffraction lines from PCL, associated with interplanar distances of 4.12 and 3.73 Å,[34] can be identified as well as a clear reduction of the crystallinity in the blends resulting from the increase in PECl content. No changes are observed in PCL peak position with blend composition, indicating as expected, that the PCL structure is not affected by the presence of the second polymer. The mass crystallinity of the blend obtained from the WAXD difractograms, X_c^{WAXD}, was calculated using the equation:

$$X_c^{WAXD} = \frac{I_c}{I_a + I_c} \qquad (8)$$

where I_c is the integrated intensity due to the crystalline PCL and I_a the integrated intensity corresponding to the amorphous component of the blend. The fitting of the curves for the determination of I_a and I_c was performed in the range $16 \leq 2\theta \leq 32$ using a logarithmic baseline for the background and Gaussian functions for the amorphous halo and the crystalline peaks.

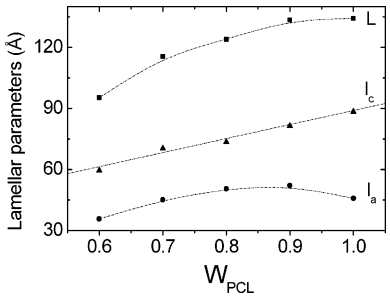

Figure 6. Average lamellar parameters as a function of PCL content. *L* long period, l_c lamellar thickness, l_a interlamellar amorphous thickness.

Table 3. Linear Crystallinity (χ_{cl}), Bulk Degree of Crystallinity (Φ_c), and Volume Fraction of Lamellar Stacks (Φ_c/χ_{cl}) of PCL/PECl Blends with Higher PCL Content

sample (PCL/PECl)	Φ_c[a]	χ_{cl}[b]	Φ_c/χ_{cl}
100/0	0.54	0.66	0.82
90/10	0.47	0.61	0.77
80/20	0.43	0.59	0.73
70/30	0.37	0.61	0.61
60/40	0.30	0.63	0.48

[a] Φ_c = bulk degree of crystallinity obtained from eq 6. [b] χ_{cl} = linear degree of crystallinity obtained from eq 7.

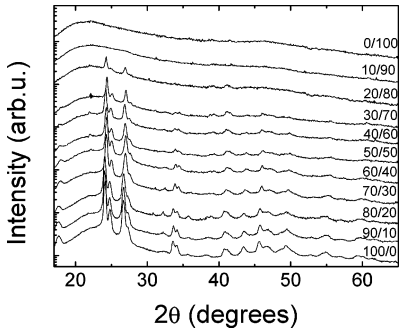

Figure 7. WAXD spectra for all PCL/PECl samples studied.

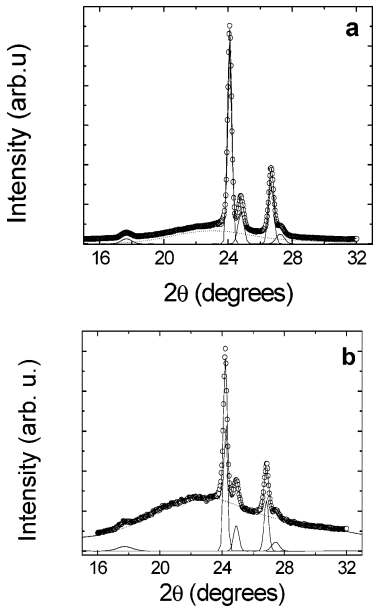

Figure 8. Typical diffractograms and fittings obtained for (a) PCL and (b) PCL/PECl (40/60) blend. Experimental data (empty dots); amorphous halo (dotted line); crystalline peaks (continuous line).

Typical fitting curves can be seen in Figure 8a,b for PCL and for the blend PCL/PECl 40/60. The addition of the PECl in the blend modifies the relative intensity between the crystalline peaks and the amorphous halo and changes the center of this contribution (halo). The results obtained using eq 8 are listed in Table 2. The agreement between WAXD and DSC calculation is remarkably good. Only the values corresponding to the more diluted samples have noticeable difference attributed to fitting errors in WAXD calculations due to the low crystalline contribution.

4. TEM. Real space observations of the morphological characteristics of the blends, in the micrometric/nanometric scale, were investigated by transmission electron microscopy. We analyzed the structural features of the crystalline regions (lamellae, lamellar bundles and spherulites) as well as the elemental maps generated by electron spectroscopy imaging (ESI) of the amorphous phase for the PCL homopolymer and the blend compositions PCL/PECl: 80/20, 60/40, 40/60, and 20/80.

All compositions show a typical spherulitic morphology. The internal regions of the spherulites (near the nucleus) for PCL show compact lamellar bundles (Figure 9a). The fibrils look dark in the bright field TEM images for PCL and the 80/20 and 60/40 blends. The latter micrographs show a progressively less compact fibrils due to the addition of PECl (Figure 9b,c).

At higher magnifications and for the more concentrated PECl compositions, individual lamellae structures are identified due to the increase in the electron density contrast between crystalline PCL and the amorphous phase that contains a much higher concentration of the chlorinated polymer (Figure 10a,b). We can also see dark regions between fibrils. These pockets of amorphous material are rich in PECl. Some smaller lamellar branches are extended into these regions.

Spherulite impingement is observed for compositions where PCL is the major component (volume filling morphology) whereas interespherulitic segregation could be seen for 40/60 and 20/80 blend compositions. In the latter case the interfaces are irregular and diffuse and isolated lamellae at the spherulitic periphery can be observed (Figure 11a,e).

5. ESI-TEM. SAXS and TEM results indicate predominant interfibrillar PECl localization when PCL is the major component in the blend. On the other hand for the 40/60 and 20/80 blends, amorphous regions with higher concentrations of chlorine are expected to be localized between spherulites. This compositional morphology can be unambiguously confirmed by electron spectroscopy imaging, mapping the chlorine distribution in those blends.

Bright-field TEM image (Figure 12a) shows a big amorphous region between spherulites (star) and darker regions inside the spherulite, in the peripheral region devoid of lamellar structures (arrow). The chlorine map shows the presence of this element in the entire image but more concentrated in the amorphous regions (Figure 12b).

Looking for the internal morphology of the blend, we observe that the Cl distribution map is also correlated with the gray regions of TEM images (Figure 13a,b). This picture is not as clear as in the former case probably due to a smaller concentration of chlorine in this region. Cl concentration in the amorphous phase depends on the region in which it is present (interlamellar, interfibrillar or interespherulitic). Similar results were reported for other blends[3] but not directly observed as in the present work.

The correlation between dark regions in TEM and rich chlorine content in elemental maps is also observed for the

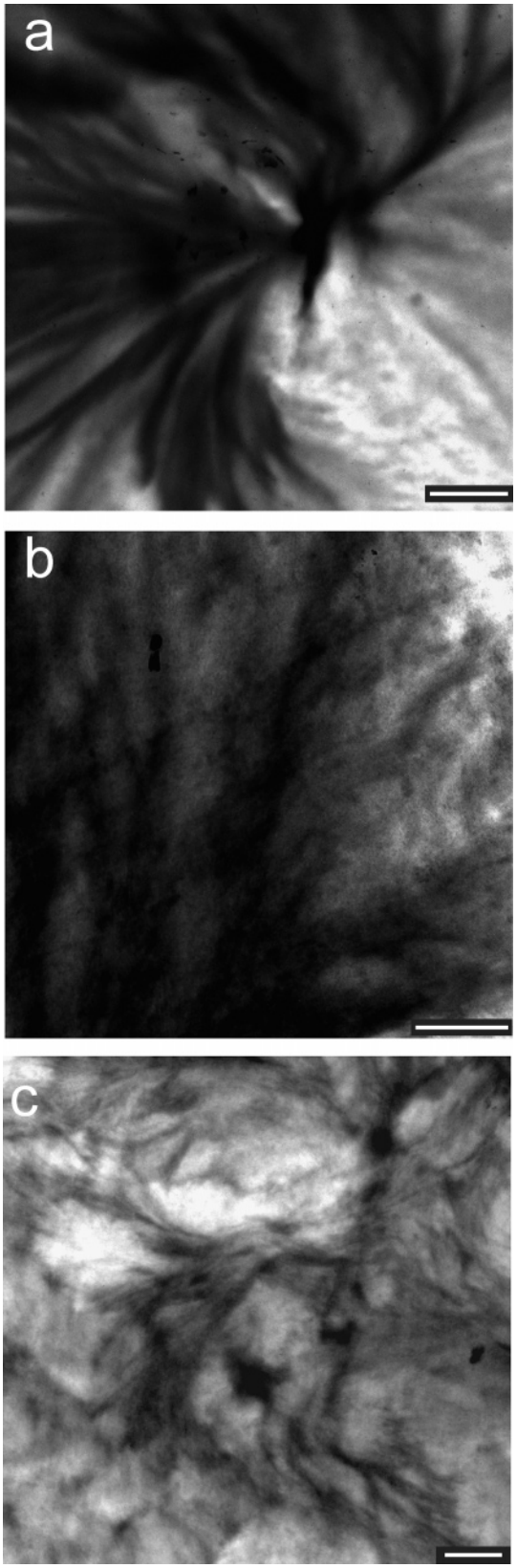

Figure 9. TEM images showing a progressively less compact morphology due to the addition of PECL in the blend: (a) PCL; (b) PCL/PECl 80/20; (c) 60/40. White bars = 1000 nm.

20/80 and 60/40 blend compositions. The blend with the higher concentration of PECl analyzed, 20/80, not only gives more evidence of the presence of rich PECl amorphous segregated regions but also reveals a chlorine concentration gradient in the interespherulitc regions (Figure 14a,b). Considering that in the

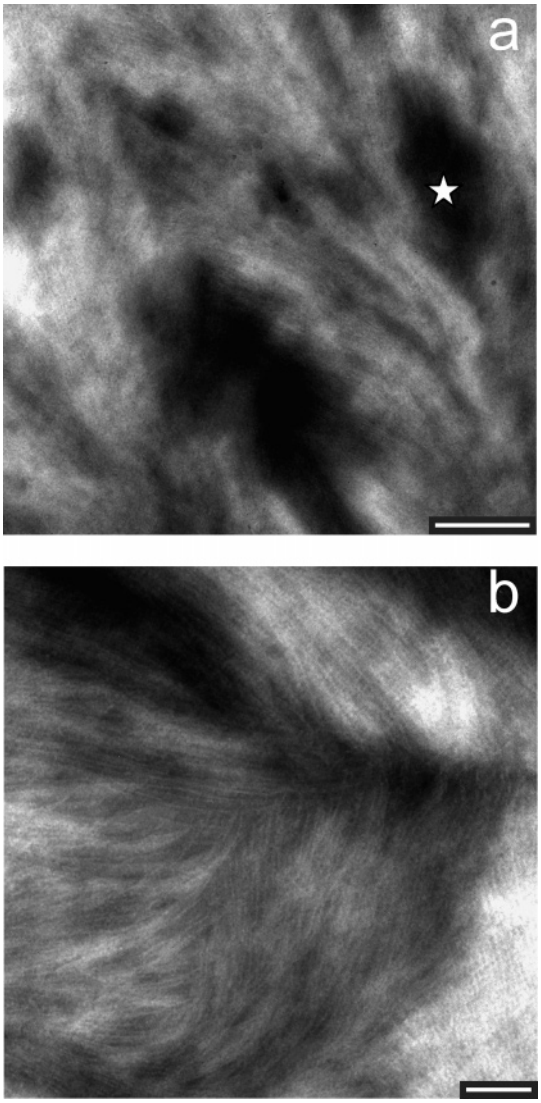

Figure 10. Morphological details at higher magnification: amorphous pocket (star) and individual lamellar structures. TEM images of (a) PCL/PECl 60/40, white bar = 500 nm; (b) 40/60 blends, white bar = 200 nm.

elemental map more intense pixels (red ones in colored picture) indicate higher concentration of one element (Cl), the plot of intensity vs distances in the selected area (2000 nm × 130 nm), clearly shows a maximum in the central part of the amorphous region (Figure 14c).

The images for the 80/20 composition are somewhat different. The chlorine rich regions are located next to the fibrils and this is expected because the growth rate of the PCL crystalline phase is fast, thus hindering PECl diffusion ahead of the spherulitic growth front. Amorphous segregation and Cl content at the point of the spherulitic impingement is minimal (Figure 15).

Discussion

Behavior of the Lamellar and Crystallinity Parameters as a Function of Blend Composition. From the results of our experiments, we confirm quantitatively that there is a real reduction in the l_c lamellar thickness with the increase of PECl content in the blend. This result was previously proposed for several blend compositions by Defideuw et al.[6] based on the variation of the long period L and the melting temperature of PCL, obtained from SAXS and DSC measurements, respec-

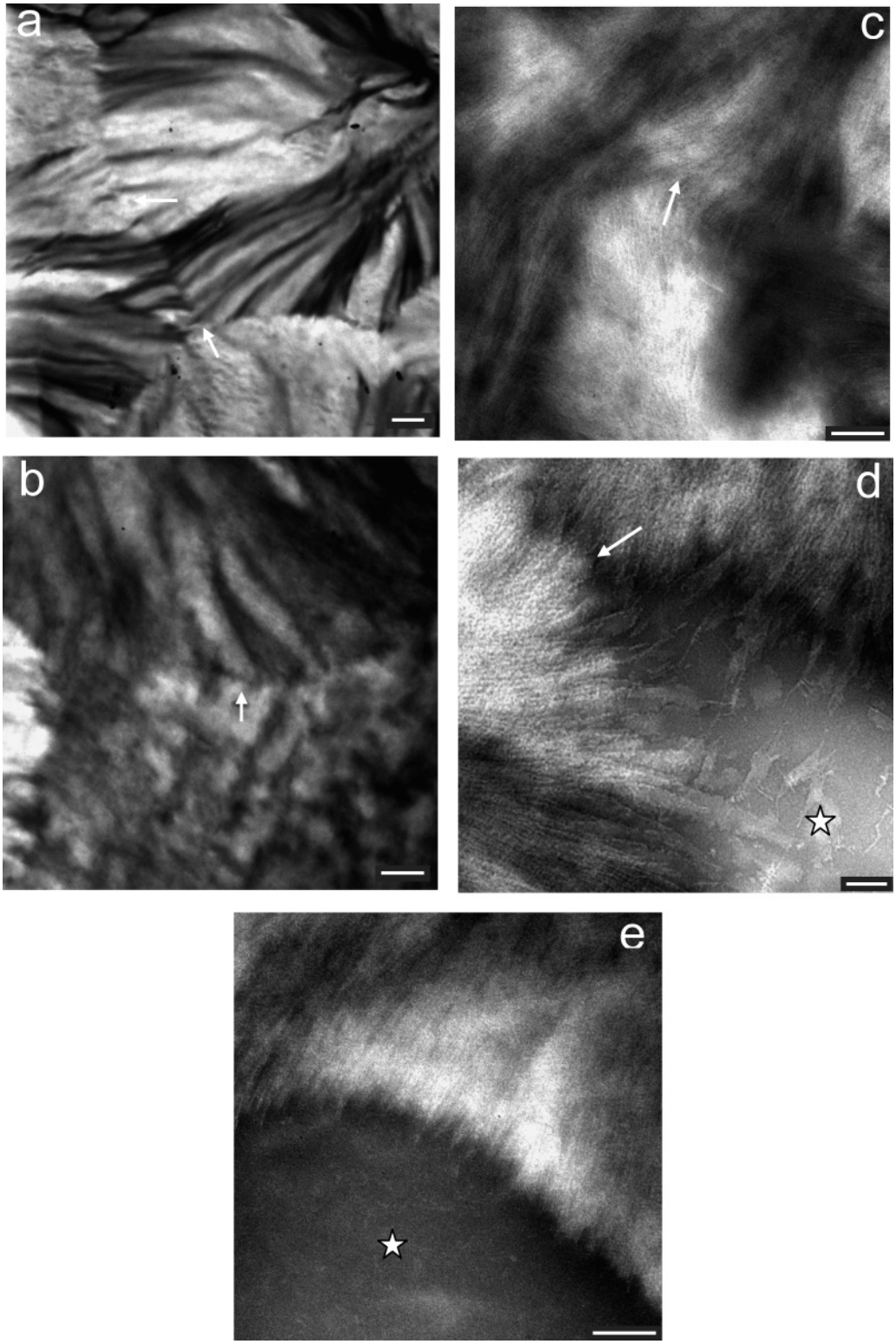

Figure 11. Interspherulitic morphology: (a) PCL; (b) PCL/PECl 80/20, white bars = 1000 nm; (c) 60/40; (d) 40/60; (e) 20/80, white bars = 200 nm. Interspherulitic interface (arrows); segregated amorphous phase (star).

tively. In this paper we clearly prove the l_c reduction by direct calculation of the one-dimensional correlation function from the SAXS data.

A more formal description of the structural changes taking place in the blends can be proposed using the secondary nucleation theory.[35,36] This theory establishes a correlation between the crystalline lamellar thickness l_c and the crystallization temperature T_c. For unlimited lateral dimensions of the crystalline lamellae and an incremental thickness factor γ for the initial crystal thickness, this relation is given by the expression:

$$l_c = \gamma\left[\frac{2\sigma_e}{\Delta H_f^\circ}\frac{T_m^\circ}{T_m^\circ - T_c} + \delta\right] \tag{9}$$

where T_m° is the equilibrium melting temperature of the blend, σ_e is the fold surface free energy, ΔH_f° heat of fusion per unit volume of the pure crystalline material, δ is the thickness that

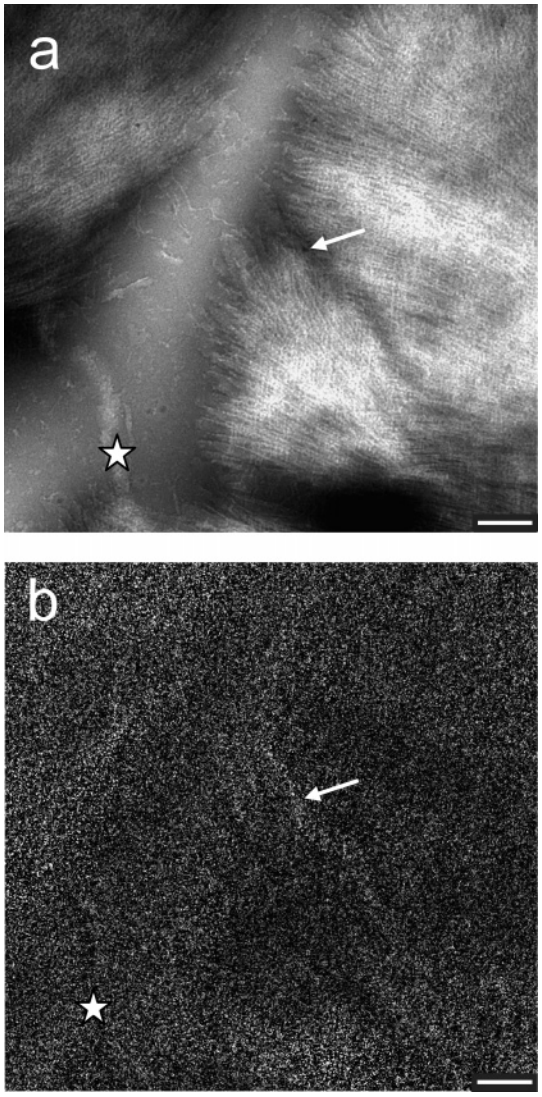

Figure 12. Chlorine rich amorphous interspherulitic regions observed for the PCL/PECl 40/60 blend: (a) bright-field TEM; (b) chlorine map. White bar = 400 nm.

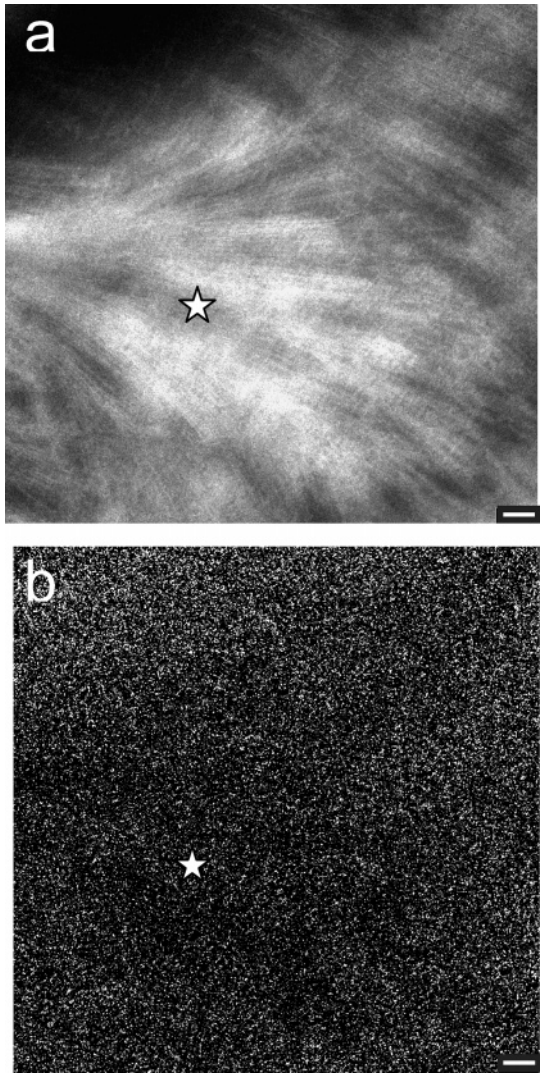

Figure 13. Chlorine rich interfibrillar regions observed for the PCL/PECl 40/60 blend: (a) bright-field TEM; (b) chlorine map. White bar = 100 nm.

gives the crystals the necessary stability to form.[37] For small to moderate values of supercooling ($T_m^\circ - T_c$), δ is negligible and the lamellar thickness is practically inversely proportional to ($T_m^\circ - T_c$), assuming γ is independent of T_c.

It is generally observed that, for the same crystallization temperature, the lamellar thickness l_c in miscible semicrystalline/amorphous blends remain unaltered or increases, when the volume fraction of the amorphous component increases. Reduction of the lamellar thickness under the same conditions has also been reported for a few systems.[2,38,39] However, the reasons for this behavior still remain under discussion.

As previously mentioned, the Flory−Huggins interaction parameter χ for this system is weak, with values close to zero. Our measurements showed that the equilibrium melting temperature of the PCL homopolymer is slightly higher than that of the PCL/PECl blend. The values obtained from Hoffman−Weeks plots are 71 °C for PCL and 68 °C for the 70/30 blend.[35,20] Thus, taking into account only the degree of supercooling, the behavior observed in Figure 6 cannot be properly explained. The solution is to consider a decrease of either γ or σ_e (or both) when the semicrystalline component (PCL) fraction in the blend decreases.

The fact that the lamellar thickness appears to depend on the interplay between the value of the free surface energy of folding and the degree of supercooling was recently pointed out by Kuo et al.[40] These authors reported a correlation between decreasing σ_e in weakly interacting blends or blends containing weak hydrogen bonds and a reduction of the lamellar thickness when the amorphous component is increased.

Determination of σ_e using the overall crystallization rate obtained from DSC data and the Hoffman−Lauritzen kinetic theory of polymer crystallization[37] shows a decrease of this parameter for larger fractions of the amorphous component in the blends ($\sigma_{e(PCL)} = 13.56 \times 10^{-2}$ J/m^2, $\sigma_{e(70/30)} = 7.75 \times 10^{-2}$ J/m^2, Plivelic et al.[41]). Consequently, reduction of l_c is a factual possibility, which at the same time indicates that σ_e is the dominant factor in the lamellar crystallization process of these blends.

TEM results show volume-filling morphology (i.e all PECl inside the spherulites) in all blends with majority mass fraction of PCL. In this case, the quotient Φ_c/χ_{cl}, is the volume fraction of lamellar stacks in the sample and a value lower than 1 could be interpreted as the existence of interfibrillar morphology. Then, the reduction of this value (see Table 3) with PECl content in the blend can be interpreted as an increase in the quantity of amorphous material segregated in the interfibrillar space. These results are coherent with the idea that PECl is not incorporated into the lamellar structure, but preferentially located into the

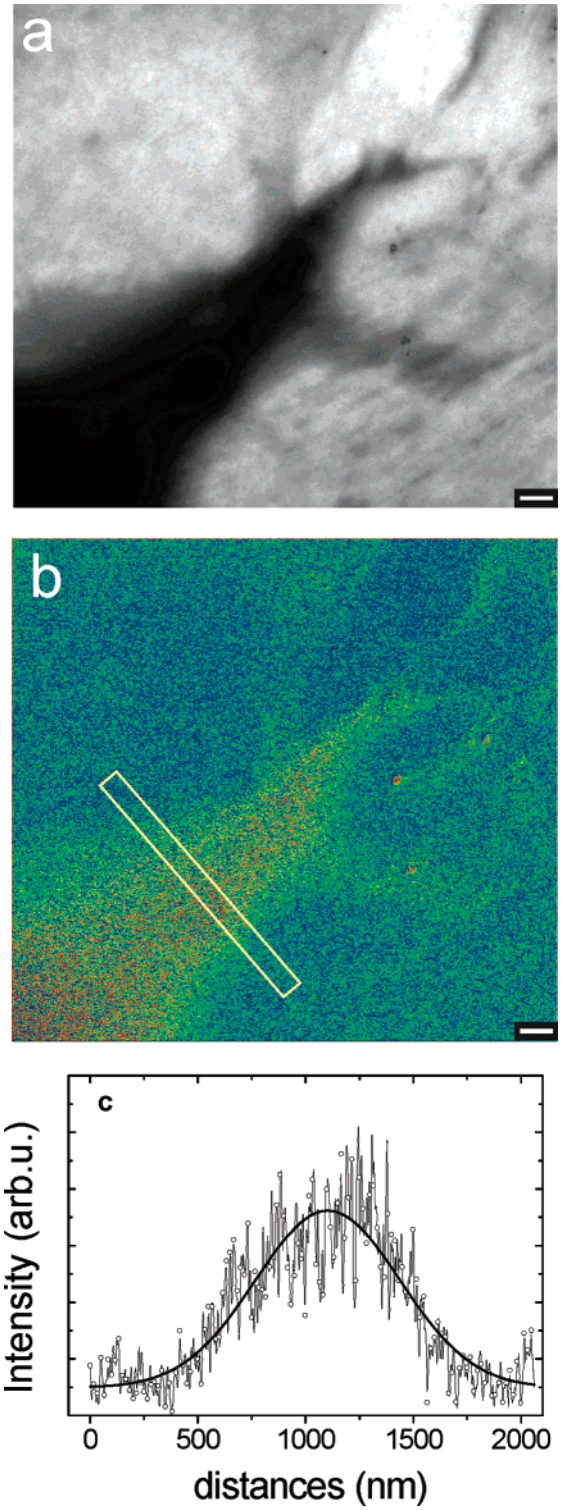

Figure 14. Gradients of chlorine concentration in larger amorphous regions of the PCL/PECl 20/80 blend: (a) bright-field TEM; (b) chlorine map, white bar = 200 nm; (c) chlorine concentration profile in the selected area (box). Continuous line: visual guide of the averaging behavior.

interfibrillar (inter lamellar branches) space. TEM images correlate very well with this idea showing a reduction in the compactness of the lamellar branches (Figure 9) when progressively more PECl is added to the blend.

Estimation of the Lamellar Thickness from TEM Pictures. An estimation of the lamellar parameters from TEM images is in general a difficult task to solve in semicrystalline/amorphous blends. In general, TEM observations and SAXS measurements

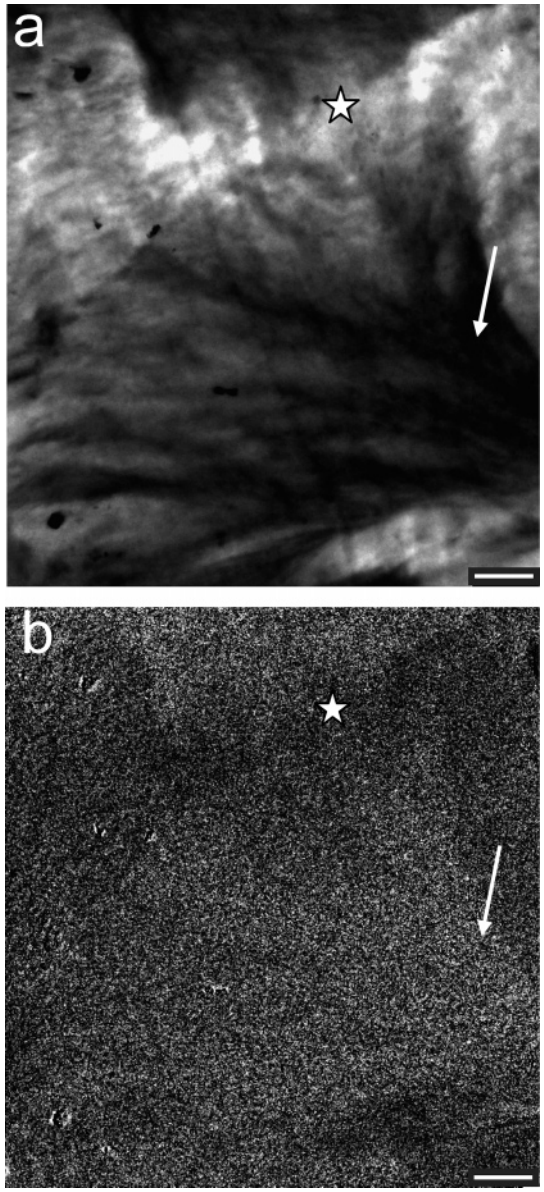

Figure 15. Chlorine localization regions in the PCL/PECl 80/20 blend: (a) bright-field TEM; (b) chlorine map. White bar = 100 nm. Key: fibrils region (arrows); spherulitic impingement region (star).

can provide useful correlations and the comparison is highly desirable.

PCL rich blends show very compact morphology and low amorphous/crystalline electronic contrast that prevent any kind of analysis. On the other hand, diluted PCL blends present isolated lamellae surrounded by large amounts of PECl that can be visualized in TEM images (i.e., Figure 11d,e). Results reported by Lovinger et al.[13] prove that no significant differences are obtained between isolated lamellae at the tips of the lamellar stacks and the lamellae in the inner part of the stacks in PEEK/PEI blends. Following this procedure we obtained a rough estimation of the lamellar thickness for 20/80, 40/60, and 60/40 PCL/PECl compositions. The program Image-Pro Plus 4.5 was used to scan the optical density of each lamella, and the average FWHM of the profiles was considered as the lamellar thickness.

The values obtained were approximately 50, 80, and 110 Å for 20/80, 40/60, and 60/40 PCL/PECl blend compositions, respectively. The values are larger than those obtained from SAXS analysis but show (in different blend composition ranges)

the same tendency of reduction of lamellar thickness with the increase of PECl content in the blend. Different values are expected considering that in ultrathin sections of bulk spherulites all lamellar orientation are possible and generally the lamellae are not perpendicular to the image plane.

Miscibility, Chlorine Concentration Gradient, and Microenvironments. It is generally known that a single compositionally dependent T_g indicates full miscibility with a dimension of the order of 20−40 nm, but it does not confirm the full miscibility of the system for smaller domain sizes.[40] The existence of complex microenvironments, different from the one expected from a simple additivity, is observed in all blend compositions. For higher W_{PCL}, the glass transition width and the heat capacity values departed from a linear behavior as a function of blend composition and SAXS results showed preferential interfibrillar localization of the amorphous component PECl. On the other hand, lower W_{PCL} blends showed different chlorine concentration depending on the localization of the amorphous components. Gradients of Cl concentration were examined by ESI-TEM in larger amorphous regions of these compositions.Microheterogeneities and preferential extralamellar segregation of the noncrystalizable polymer are mainly a consequence of the weak Flory−Huggins interaction parameter for the polymer blend under study.

Conclusions

DSC results confirm the existence of a unique glass transition temperature in each blend. The heat capacity and the width of the glass transition do not have a linear behavior with blend compositions suggesting the existence of microheterogeneities with different local compositions and densities of interactions in each blend. For the annealed samples, the degree of crystallinity of PCL remains practically constant for all compositions up to 20% of PCL. The crystallization process measured during cooling of the system from the melted state shows lower T_c values when more PECl is added to the blend, indicating that PCL crystallization is hindered by the presence of the amorphous diluent in the blend.

As expected for a miscible semicrystalline/amorphous polymer blend, the structure of the semicrystalline polymer is not affected by the presence of the other component. The values of the degree of crystallinity of the blends obtained by X-ray diffraction data and DSC measurements are in good agreement. This result and the combined SAXS/WAXD measurements in the same sample provide a reliable and consistent picture of the system under analysis.

The overall small-angle X-ray scattering curves of the blends are characterized by the superposition of a monotonically decreasing profile due to inhomogeneities of the amorphous phase and a correlation peak associated with the lamellar periodicity. The one-dimensional correlation function calculated from the SAXS curves, corrected by subtraction of the melted state curve of each blend composition, clearly proves the reduction of the long period and the lamellar thickness (l_c) with the increase of PECl content in the blend (for the higher W_{PCL}). l_c reduction could be rationalized if the free surface energy of folding is the dominant factor over the degree of supercooling in the crystallization process. Such behavior fits very well with the generic relation proposed for l_c and σ_e in weakly interacting blends.[40]

The volume fraction of lamellar stacks obtained by simultaneous SAXS/WAXD data decrease with the increase of PECl content in the blend, and the result can be interpreted as an increase in the quantity of amorphous material segregated in the interfibrillar space. TEM images correlate very well with this idea.

Transmission electron microscopy images show that the spherulitc morphology of PCL is observed in all blend compositions. This structure becomes more irregular and coarser when PECl is added in the blend. In PCL-rich blends, only dense lamellar branches could be identified whereas for 60/40, 40/60, and 20/80, the individual lamellae could be clearly seen due to the increase in the electron density contrast between crystalline PCL and the amorphous phase rich in PECl. The predominant PECl distribution is between fibrils. Most lamellae tend to grow tightly packed avoiding interlamellar inclusion of the amorphous component. Such tendency was also observed for PEEK in the PEEK/PEI blends[42] and isotactic polystyrene in isotactic/atactic polystyrene blends.[43] The origin of this trend was justified by the structure of the noncrystalline regions at the vicinity of a crystal surface, which favor the growth of a close parallel lamella.[3]

Blends with higher content of PECl (W_{PCL} lower that 50%) shows interespherulitic segregation. This preferential localization of the amorphous component is related to the drastic reduction of the growth rate with the composition of the blend, which allows the diffusion of PECl ahead of the spherulitic growth front.

Elemental images demonstrate the successful imaging of PCL/PECl blends without further treatment (e.g., staining or etching). Unambiguous chlorine localization is established, showing that extralamellar amorphous regions are chlorine rich. This fact is more clearly visualized when there is interespherulitc segregation of PECl (40/60 and 20/80 blend compositions). Gradients of chlorine concentration are also measured by ESI-TEM in larger amorphous regions of these compositions. The composition with higher PCL content (80/20) shows PECl very near the lamellar branches and fully inside of the spherulites.

Acknowledgment. This work has been supported by the Brazilian Synchrotron Light Source (LNLS) under proposal D11A/SAXS #1709 and the Research Foundation FAPESP, Brazil. We thank Carlos A. Leite for the assistance with the ESI-TEM images and Adair Rangel de Oliveira, Jr., for the assistance with TEM sample preparation, Gerson Mantovani for the measurements of the average molecular weights of the homopolymers and the ^{13}C solid state RMN of PECl, and M. I. Felisberti for the DSC measurements performed at the Institute of Chemistry,UNICAMP.

References and Notes

(1) Debier, D.; Jonas, A. M.; Legras, R. *J. Polym Sci. B: Polym. Phys.* **1998**, *36*, 2197−2210.
(2) Cheng, H. L.; Li, L. J.; Lin, T. L. *Macromolecules* **1998**, *31*, 2255−2264.
(3) Jonas, A. M.; Ivanov, D. A.; Yoon, D. Y. *Macromolecules* **1998**, *31*, 5352−5362.
(4) Talibuddin, S.; Wu, L.; Runt, J.; Lin, J. S. *Macromolecules* **1996**, *29*, 7527−7535.
(5) Bélorgey, G.; Prud'homme, R. E. *J. Polym. Sci., Polym. Phys. Ed.* **1982**, *20*, 191−203.
(6) Defieuw, G.; Groeninckx, G.; Reynaers, H. *Polymer* **1989**, *30*, 595−603.
(7) Calandrelli, L.; Immirzi, B.; Malinconico, M.; Volpe, M. G.; Oliva, A.; Della Ragione, F. *Polymer* **2000**, *41*, 8027−8033.
(8) Pitt, C.G.; Jeffcoat, A. R.; Zweidinger, R. A.; Schindler, A. *J. Biomed. Mater. Res.* **1979**, *13*, 497−507.
(9) Wang, Z. G.; Hsiao, B. S.; Fu, B. X.; Liu, L.; Yeh, F.; Sauer, B. B.; Chang, H.; Schultz, J. M. *Polymer* **2000**, *41*, 1791−1797.
(10) Huang, C. I.; Chen, J. R. *J. Polym. Sci., Polym. Phys. Ed.* **2001**, *39*, 2705−2715.
(11) Shabana, H. M.; Olley, R. H.; Bassett, D. C.; Jungnickel, B. J. *Polymer* **2000**, *41*, 5513−5523.

(12) Crevecouer, G.; Groeninckx, G. *Macromolecules* **1991**, *24*, 1190−1195.
(13) Hudson, S. D.; Davis, D. D.; Lovinger, A. J. *Macromolecules* **1992**, *25*, 1759−1765.
(14) Lisowski, M. S.; Liu, Q.; Cho, J.; Runt, J.; Yeh, F.; Hsiao, B. S. *Macromolecules* **2000**, *33*, 4842−4849.
(15) Ivanov, D. A.; Lipnik P. D. M.; Jonas A. M. *J. Polym. Sci., Polym. Phys.* **1997**, *35*, 2565−2570.
(16) Eastmond, G. C. *Adv. Polym. Sci.* **2000**, *149*, 59−223.
(17) Svoboda, P.; Kressler, J.; Chiba, T.; Inoue, T.; Kammer, H. W. *Macromolecules* **1994**, *27*, 1154−1159.
(18) Torriani, I. L.; Oliveira, C. L. P.; Dos Santos, D. R.; Neuenschwander, R.; Kellermann, G.; Plivelic, T. S. *Abstracts of the "SAS-99 International Conference"*; Brookhaven, NY, 1999; p 298.
(19) Bras, W.; Derbyshire, G. E.; Devine, A.; Clark, S. M.; Komanschek, B. E.; Ryan, A. J. *J. Appl. Crystallogr.* **1995**, *28*, 26−32.
(20) Plivelic, T. S.; Cassu, S. N.; Gonçalves, M. C.; Torriani, I. L. *Polím.: Ciên. Tecnol.* **2005**, *15*, 199−206.
(21) Fox, T. G. *Bull. Am. Phys. Soc* **1956**, *1*, 123.
(22) Fernandes, A. C.; Barlow, J. W.; Paul, D. R. *J. Appl. Polym. Sci.* **1984**, *29*, 1971−1983.
(23) Guo, Q.; Harrats, C.; Groeninckx, G.; Reynaers, H.; Koch, M. H. J. *Polymer* **2001**, *42*, 6031−6041.
(24) Khambatta, F. B.; Warner, F.; Russell, T.; Stein, R. S. *J. Polym. Sci., Polym. Phys. Ed.* **1976**, *14*, 1391−1424.
(25) Cassu, S. N.; Felisberti, M. I. *Polymer* **1997**, *38*, 3907−3911.
(26) Song, M.; Hammiche, A.; Pollock, H. M.; Hourston, D. J.; Reading, M. *Polymer* **1995**, *36*, 3313−3316.
(27) Shen, S.; Torkelson, J. M. *Macromolecules* **1992**, *25*, 721−728.
(28) Hutchinson, J. M. In *The physics of glassy polymers*, 2nd ed.; Haward, R. N., Young, R. J., Eds.; Chapman & Hall, London, 1997; pp 105, 128.
(29) Goderis, B.; Reynaers, H.; Koch, M. H. J.; Mathot, V. B. F. *J. Polym. Sci., Polym. Phys. Ed.* **1999**, *37*, 1715−1738.
(30) Strobl, G. R.; Schneider, M. *J. Polym. Sci. Polym. Phys. Ed.* **1980**, *18*, 1343−1359.
(31) Huo, P. P.; Cebe, P.; Capel, M. *Macromolecules* **1993**, *26*, 4275−4282.
(32) Russell, T. P.; Stein, R. S. *J. Polym. Sci., Polym. Phys. Ed.* **1982**, *20*, 1593−1607.
(33) DeLassus, P. T.; Whiteman, N. F. In *Polymer Handbook*, 4th ed.; Brandrup, J., Immergut, E. H., Grulke, E. A., Eds.; John Wiley & Sons: New York, 1999; Chapter 5, p 169.
(34) Walsh, D.; Furuzono, T.; Tanaka, J. *Biomaterials* **2001**, *22*, 1205−1212.
(35) Hoffman, J. D.; Weeks, J. J. *J. Res. Natl. Bur. Stand., Sect. A* **1962**, *66*, 13.
(36) Hoffman, J. D.; Davis, G. T.; Lauritzen, J. I. In *Treatise on Solid State Chemistry*; Hanay, N. B., Ed.; Plenum Press: New York, 1976; Vol. 3, p 497.
(37) Hoffman, J. D.; Miller, R. L. *Polymer* **1997**, *38*, 3151−3212.
(38) Wenig, W.; Karasz, F. E.; MacKnight, W. J. *J. Appl. Phys.* **1975**, *46*, 4194−4198.
(39) Oudhuis, A. A. C. M.; Thiewes, H. J.; van Hutten, P. F.; t Brinke, G. *Polymer* **1994**, *35*, 3936−3942.
(40) Kuo, S. W.; Chan, S. C.; Chang, F. C. *Macromolecules* **2003** *36*, 6653−6661.
(41) Plivelic, T. S.; Cassu, S. N.; Gonçalves, M. C.; Torriani, I. L. Work in progress.
(42) Lovinger, A. J.; Hudson, S. D.; Davis, D. D. *Macromolecules* **1992**, *25*, 1752−1758.
(43) Vaughan, A. S. *Polymer* **1992**, *33*, 2513−2521.

MA061265M